Journal of Solid State Chemistry 181 (2008) 2953–2963

Contents lists available at ScienceDirect

Journal of Solid State Chemistry

journal homepage: www.elsevier.com/locate/jssc

Effect of the rare earth in the perovskite-type mixed oxides $A\mathrm{MnO_3}$ (A = Y, La, Pr, Sm, Dy) as catalysts in methanol oxidation

B. Levasseur, S. Kaliaguine *

Department of Chemical Engineering, Laval University, Sainte-Foy, Que., Canada G1K 7P4

ARTICLE INFO

Article history:
Received 16 April 2008
Received in revised form
21 July 2008
Accepted 24 July 2008
Available online 30 July 2008

Keywords:
Perovskite
Rare earth
Methanol oxidation
Thermodesorption experiments
Electronegativity
Carbonates

ABSTRACT

The effect of the rare earth in the perovskite-type mixed oxides $A\mathrm{MnO_3}$ (A = Y, La, Pr, Sm, Dy) on catalytic properties in methanol oxidation was investigated in this work. The perovskites were prepared by reactive grinding in order to enhance the specific surface area in comparison with other classical synthesis procedures. These catalysts were characterized by N_2 adsorption, X-ray diffraction, H_2 temperature-programmed reduction (TPR-H_2), O_2-, CH_3OH- and CO_2-temperature-programmed desorption (TPD). The activity of the five catalysts under study in the methanol oxidation reaction was evaluated. The behaviour of the α-O_2 from the surface of the perovskite was strongly related to the nature of the A-site cation and particularly to its electronegativity but also to its density. Concerning the β-O_2 from the bulk, the rare earth only induces an indirect effect notably due to structural modifications. As suggested in a previous study, the activity in methanol oxidation was directly linked with the surface oxygen density. Under an excess of α-oxygen, the reaction intermediate was found to be a monodentate carbonate that decomposes into CO_2. The stability of monodentate carbonates was also found to be related to the electronegativity of the rare earth during both CH_3OH- and CO_2-temperature-programmed desorption. However, as soon as a lack of α-oxygen was observed in the structure, the dominant reaction intermediate was a bidentate carbonate that induces a consumption of anion vacancies in spite of the production of CO_2. Nevertheless, the accumulation of these carbonates leads to a decrease in the oxidation rate since their desorption requires high temperatures.

1. Introduction

Owing to their efficiency towards the oxidation of hydrocarbons and volatile organic compounds, the perovskite-type mixed oxides were extensively studied for the last four decades. Those oxides with ABO_3 formula were even suggested as an alternative to the metal-supported catalysts [1–6]. However, their low specific surface area was often considered as a major impediment to their use. Thus, numerous synthesis procedures were developed to enhance the specific surface area including coprecipitation [7], citrate complexation [8], spray drying [3], freeze drying [9] and flame hydrolysis [10]. Nevertheless, the specific surface area observed on perovskites prepared by these methods rarely exceeds 25 m^2/g. The calcination step required for the crystallization of the perovskite phase is considered detrimental. Indeed the high temperature used during the calcination induces a decrease in specific surface area through a severe sintering process. Reactive grinding (RG) was developed with the purpose of replacing the thermal energy required for the crystallization by a mechanical treatment that allows the preparation of mixed oxides at rather low temperatures [11]. The materials prepared by RG present nanometric-size particles and large specific surface areas, which can exceed 100 m^2/g [12]. The Québec firm Nanox Inc. has installed a demonstration unit of RG for the production of perovskite with a capacity of 15 t/year.

The role of the rare earth in the perovskite structure is not really clear and is still being discussed. Nitadori et al. have studied the effects of A-site cation. These authors show significant differences in the perovskite structure, whereas the reducibility and the behaviour of the oxygen of the solid have not been really affected [13]. In terms of activity, the CO oxidation was reported to be easier with Nd and Ho in the $Ln\mathrm{CoO_3}$ (Ln = La, Pr, Nd, Gd and Ho) structure [14] while at the same time no real influence was observed on methane oxidation [15]. The effect of partial substitution of the rare earth in the perovskite structure was well discussed in the literature. Indeed numerous studies reported partial substitution of La by Sr or Ce. It seems that such a substitution acts like a valence control in the structure and leads to a significant enhancement of reducibility [16] and an increase in surface oxygen desorption during TPD-O_2 [13]. An

* Corresponding author. Fax: +1 418 656 3810.
E-mail address: serge.kaliaguine@gch.ulaval.ca (S. Kaliaguine).

0022-4596/$ - see front matter © 2008 Published by Elsevier Inc.
doi:10.1016/j.jssc.2008.07.029

increase of the activity in CH_4 and CO oxidations was also observed on $La_{1-x}Sr_xMnO_3$ until $x = 0.2$ and $La_{1-x}Ce_xMnO_3$ until $x = 0.1$ [17].

The partial or total oxidation of methanol represents a great interest for industrial chemistry. The industrial gas pollutant treatment and the elimination of exhaust effluents produced by alcohol-fueled vehicles are among the applications of the total oxidation of methanol [18]. Metallic catalysts, especially Pt and Pd, have shown a great efficiency for total methanol oxidation [18,19] whereas the molybdenum-based catalysts are efficient towards the partial methanol oxidation [20–23]. The effect of *A*-site cation in this reaction has been studied for manganites and ferrites perovskites [24,25]. Even if the authors suggest that the rare-earth nature induces a modification of the covalent M–O bond, only slight differences were observed in the total methanol oxidation reaction.

This study deals with the effect of the *A*-site cation in the structure and especially for the oxidation of methanol. Five manganites perovskite-type mixed oxides were synthetized by RG. Both structural (S_{BET} and X-ray diffraction) and redox characterizations (TPR-H_2 and TPD-O_2) were carried out on these solids. TPD-CH_3OH and TPD-CO_2 were used to evaluate the impact of the rare earth in the structure on adsorption of a reactant and product of the total methanol oxidation.

2. Experimental

2.1. Catalysts preparation

Five samples of perovskites-type materials were prepared, by RG ($LaMnO_3$, $YMnO_3$, $PrMnO_3$, $SmMnO_3$ and $DyMnO_3$). They were synthetized from the single oxides. The precursors were first calcined at 600 °C and then introduced in a SPEX laboratory grinder for a first grinding during 4 h under O_2. After this step, the perovskite phase was obtained but a second grinding was performed in order to increase the specific surface area [12]. Thus, ZnO was introduced as an additive in a weight ratio perovskite/ZnO = 1. Then the obtained powder was repeatedly washed with diluted NH_4NO_3 in order to leach out the additive from the sample. Finally, the perovskite was calcined under air at 550 °C for 6 h.

2.2. Catalysts characterization

Surface specific areas were obtained from adsorption/desorption isotherms of N_2 at −196 °C determined using an OMNISORB apparatus. Before adsorption, the samples were first evacuated for 6 h at 200 °C to remove moisture. The specific surface area was then determined from the linear part of the BET curve. The crystalline phases identification was performed by X-ray diffraction using a SIEMENS D5000 diffractometer and Cu$K\alpha$ radiation ($\lambda = 1.5406$ Å). Diffractograms were recorded with a step of 0.05° for 2θ between 15° and 75°. Phase recognition was made by comparison with JCPDS files. Particle sizes (D) were evaluated by means of the Scherrer equation $D = K\lambda/(\beta \cos\theta)$ after Warren's correction for instrumental broadening. K is a constant equal to 0.86 and λ is the wavelength of the X-ray used. β is the effective linewidth of the X-ray reflexion, calculated by the formula $\beta_2 = B^2 - b^2$, where B is the FWHM and b is the instrumental broadening determined by the FWHM of the X-ray reflection of SiO_2, having particles larger than 150 nm, at $2\theta \approx 27°$. Sample compositions were determined by ICP using a P40 atomic adsorption spectrometer from Perkin-Elmer after dissolution of the catalyst in diluted HCl at 60 °C.

2.3. TPD–TPR characterization

An RXM-100 multi-catalyst testing and characterization system (Advanced Scientific Design Inc.) was used to perform oxygen, carbon dioxide and methanol thermodesorption (TPD-O_2, TPD-CO_2 and TPD-CH_3OH) and temperature-programmed reduction (TPR). For TPR experiments, 100 mg of catalysts were placed in a quartz reactor, pretreated under a flow of 20 mL/min (20% O_2 in He) at 550 °C for 2 h and cooled down to room temperature under the same composition flow. The TPR was carried out under a 10 mL/min flow rate of 5% H_2 in Ar. The temperature was increased from 25 to 900 °C with a ramp of 5 °C/min. The consumption of hydrogen was monitored and quantified using a TCD. For TPD-O_2, the same pretreatment was performed as for the TPR experiments. The catalysts (100 mg) were submitted to the following conditions: 10 mL/min He, temperature from 25 to 900 °C with a ramp of 5 °C/min. To obtain a complete desorption, the catalysts were maintained at 900 °C for 15 min. A TCD was used for the quantification of oxygen and a mass spectrometer was used to detect any other compounds' desorption or possible leaks. The amount of oxygen was determined by deconvolution and integration of the desorption profile. To perform a TPD-CH_3OH or TPD-CO_2, two steps were required. During the first step, the catalysts (100 mg) were calcined in the same conditions as for TPR experiments. Then the catalysts were treated under 15% CH_3OH in He or under CO_2 at room temperature for 1 h. Thereafter, the methanol thermodesorption was carried out under 10 mL/min flow of He from 25 to 900 °C with a ramp of 5 °C/min followed by an isotherm at 900 °C for 15 min. Like TPD-O_2, TCD and mass spectrometer were used to quantify and identify the desorbed species.

2.4. CH_3OH oxidation reaction

Methanol oxidation was performed in a U-shaped quartz reactor (i.d. = 5 mm). The catalytic bed was set up with 100 mg of catalysts inserted between two quartz wool plugs. The temperature was controlled using a K-type thermocouple placed in the reactor. In order to purge the catalytic system, the catalysts were flushed with a 20 mL/min flow of He for 1 h at room temperature. The feed, composed of 0.5% CH_3OH, and 5% O_2 in He, was passed through the reactor and the temperature was increased. The flow rate was adjusted to 30 mL/min, which corresponds to a VHSV of 22,500 h^{-1}. Gas samples were collected in the steady-state regime at various reaction temperatures and the products were analyzed with a gas chromatograph (HP 6890 series), equipped with a TCD. Reactants and products were separated using a HayeSep T column (i.d. = 1 mm, $L = 2\,m \times 5\,m$).

3. Results

3.1. Physical properties

Table 1 summarizes the chemical composition, BET surface area and crystallite size of the $AMnO_3$ perovskites prepared by RG. The X-ray diffraction patterns of the five perovskites under study are shown in Fig. 1. The perovskite structure was the only one observed for each solid in the XRD diffractograms with their respective crystal structures (rhombohedral for LaMn-RG and orthorhombic for the others). For LaMn-RG catalysts, the comparison with the JCPSD card 50-0298 suggests the formula $LaMnO_{3.15}$, which presents an oxygen excess. This excess of oxygen in the $LaMnO_{3+\delta}$ structure was often observed after calcination under air. Such a feature was already noticed in the literature, and a number

Table 1
Physical properties of $AMnO_3$ catalysts

Samples	Chemical composition	S_{BET} (m^2/g)	Crystallite size (nm)	S_{Th} (m^2/g)	R (S_{Th}/S_{BET})
LaMn-RG	$La_{0.98}Mn_{0.99}O_3$	41	11.8	69.7	1.70
YMn-RG	$Y_{1.02}Mn_{0.99}O_3$	37	13.3	61.9	1.67
PrMn-RG	$Pr_{1.01}Mn_{0.97}O_3$	35	13.4	61.4	1.75
SmMn-RG	$Sm_{0.99}Mn_{1.01}O_3$	34	13.1	62.8	1.85
DyMn-RG	$Dy_{0.99}Mn_{0.98}O_3$	32	13.5	60.9	1.91

S_{Th}, specific surface area calculated assuming cubic particles and a density of perovskite equal to 7.29 g/cm^3.

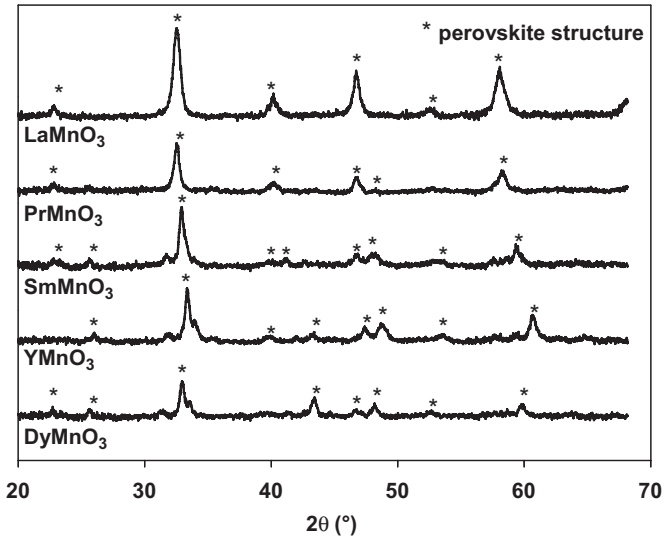

Fig. 1. X-ray diffraction patterns of the $AMnO_3$ catalysts.

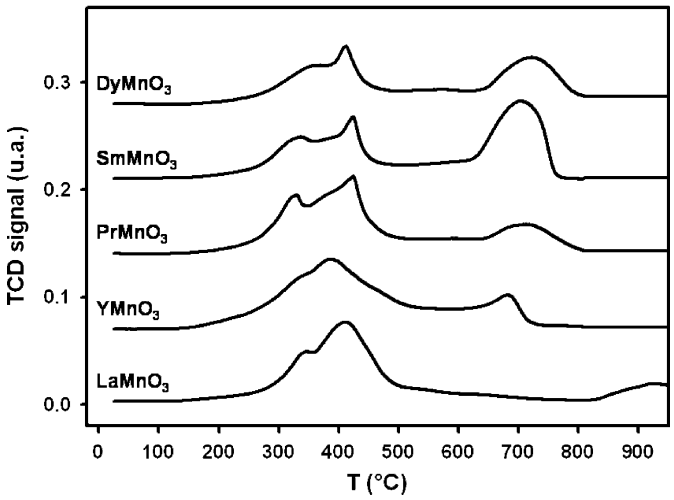

Fig. 2. H_2-TPR profiles of $AMnO_3$ perovskites.

of studies agreed for a δ value between 0.15 and 0.17 [26,27]. In this work, the amount of oxygen in the manganese-based perovskites was assumed to be 3.15. A fraction of manganese (around 25%) of valence +4 is the direct consequence of the over-stoichiometry in oxygen observed on these manganese-based oxides.

The specific surface areas measured on the five ground perovskites under study was comprised between 41 m^2/g (LaMn-RG) and 32 m^2/g (DyMn-RG). Their particle diameters calculated by the Scherrer equation from XRD lines after Warren's correction for instrumental broadening were found to vary between 11.8 nm (LaMn-RG) and 13.5 nm (DyMn-RG). With the exception of LaMn-RG no clear difference was noticed between the particle sizes of the other catalysts. The large differences observed between the specific surface areas measured by BET and those determined from the diameters evaluated from the X-ray line broadening indicate that the nanoparticles are not separated. As previously reported, the clustering of those elemental nanoparticles confers a porous structure to the ground perovskites [28–30].

3.2. TPR by H_2 (TPR)

Redox abilities of the five catalysts under study were evaluated by TPR by H_2 (TPR-H_2). The results of these reductions are shown in Fig. 2 and the evaluations of the H_2 uptake at low and high temperatures of reduction are reported in Table 2. Two major peaks of reduction were detected on each perovskite. Furthermore, a weaker signal was also differentiated on each profile at low temperature before the first peak of reduction. It was materialized by a small peak on PrMn-RG (333 °C) and SmMn-RG (340 °C) and by a shoulder on the three other catalysts. On LaMn-RG, two major signals were observed at 417 °C and over 900 °C for a total H_2 uptake of 0.67 mol H_2/mol Mn. This H_2/Mn ratio higher than 0.5 suggests the presence of another form of Mn than Mn^{3+} in the lattice. In the literature, overstoichiometric oxygen in the lanthanum manganite (still suggested in our case by XRD patterns) was often associated with the presence of Mn^{4+} in the lattice of the $LaMnO_3$ perovskite [30,31]. Besides, the presence of this species has also been noticed with other rare earth than La [16]. Thus, two successive steps occur during the reduction process: the first one that is the reduction of the $Mn^{(IV)}$ into $Mn^{(III)}$ and the second one that corresponds to the reduction until the $Mn^{(II)}$ form. There complete reduction until the state $Mn^{(0)}$ does not occur. Due to its low cation coordination number in the perovskite lattice, the Mn^{4+} species is easily reduced at low temperatures. This is likely associated with the shoulder observed at 340 °C on LaMn-RG [32].

Based on the total H_2 uptake evaluated on the four other catalysts, this two-step process of reduction should occur regardless of the *A*-site cation in the structure.

According to the previous observations, the weak signal observed at low temperature was ascribed to the reduction of the $Mn^{(IV)}$ into $Mn^{(III)}$ [31,32]. The amount of $Mn^{(IV)}$ was evaluated for each catalyst, based on the deconvolution of the minor peak observed at the lowest temperatures (Table 2). Besides, the reducibility of the $Mn^{(III)}$ should depend on its position in the structure. Indeed it may be suggested that the $Mn^{(III)}$ on the surface should be more easily reduced compared with the one in the lattice. Thus, the first peak should be ascribed to the reduction of the surface $Mn^{(III)}$ and the second signal observed at higher

Table 2
Amounts of H_2 uptake determined by TPR on $AMnO_3$ catalysts

Samples	H_2 uptake at low T/mol H_2/mol Mn (T_{max}/C)[a]		H_2 uptake at high T/mol H_2/mol Mn (T_{max}/C)[a]	$Mn^{(IV)}/Mn_{tot}$	Excess-O_2 (μmol/g)[b]	Experimental formula
LaMn-RG	0.19 (347)	0.41 (417)	0.11 (910)	0.27	564.5	$LaMn^{4+}_{0.27}Mn^{3+}_{0.73}O_{3.14}$
YMn-RG	0.15 (349)	0.42 (393)	0.10 (683)	0.22	576.1	$YMn^{4+}_{0.22}Mn^{3+}_{0.78}O_{3.11}$
PrMn-RG	0.11 (333)	0.27 (427)	0.17 (720)	0.19	399.9	$PrMn^{4+}_{0.19}Mn^{3+}_{0.81}O_{3.10}$
SmMn-RG	0.09 (344)	0.21(426)	0.33 (711)	0.14	282.3	$SmMn^{4+}_{0.14}Mn^{3+}_{0.86}O_{3.07}$
DyMn-RG	0.05 (367)	0.23 (413)	0.24 (727)	0.10	203.6	$DyMn^{4+}_{0.10}Mn^{3+}_{0.90}O_{3.05}$

[a] Calculated by deconvolution, with Lorentzian fit, of the H_2 uptake curves.
[b] Evaluation based on the $Mn^{(IV)}/Mn_{tot}$ ratio.

temperature to the reduction of the lattice $Mn^{(III)}$. However, it seems possible to obtain in some cases the reduction of the lattice

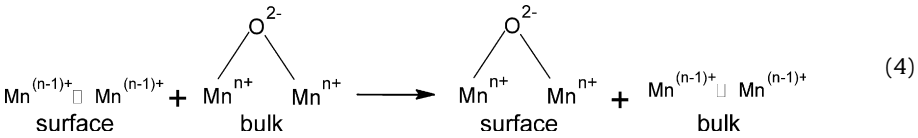

(4)

$Mn^{(III)}$ at low temperature, as noticed with LaMn-RG, YMn-RG and PrMn-RG, which present only a weak signal at higher temperature.

3.3. Temperature-programmed desorption of O_2 (TPD-O_2)

The literature reports two kinds of desorbed oxygen species, which correspond to two peaks in the TPD-O_2 profiles of perovskite-type oxides. The first kind is designated as α-O_2 and it desorbs below 700 °C. It is considered as a surface species [12] and its desorption is represented by Eq. (1):

(1)

or Eq. (2):

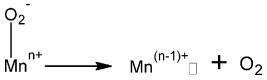

(2)

The desorption temperature of α-O_2 is strongly dependent on the temperature of calcination so that when calcination is performed at 550 °C oxygen desorption peaks are observed at 600–650 °C. At these temperatures, it is very likely that the molecular O_2^- species dissociates into atomic species. Since however this dissociation is reversed during the desorption process, the α-O_2 desorption may still be depicted by Eqs. (1) or (2).

α-O_2 have been divided into two subgroups [28] with the low temperature desorbing one being designated as α_1-O_2 and the one desorbing above 500 °C as α_2-O_2. The amount of α_1-O_2 and α_2-O_2 desorbed from the five perovskite materials is reported in Table 3.

The second peak, detected above 750 °C, is ascribed to the β-O_2, which originates from the bulk of the structure and is often considered as an indicator of the mobility of the oxygen in the structure. This desorption requires the formation of the β-O_2 desorption site [12]:

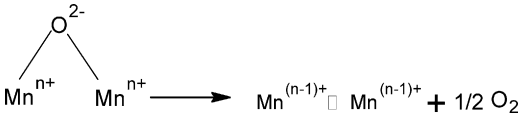

(3)

This step is followed by the diffusion of β-oxygen from the bulk to the desorption site at the surface of the structure:

Fig. 3 presents the TPD-O_2 profiles of the five catalysts under study and Table 3 summarizes the amounts of oxygen desorbed from these catalysts. The α_1-O_2 desorption occurs under 500 °C on the five catalysts under study whereas the range of temperature for the desorption of the α_2 oxygen is comprised between 630 °C for YMn-RG and 680 °C for LaMn-RG. The evaluation of the amount of α_1-O_2 and α_2-O_2 desorbed was calculated by deconvolution of the O_2 desorption curves (using Lorentzian peak shapes in a computer peak-fitting routine). The amount desorbed from the surface (α_1-O_2) on each catalysts is very low, under 22.2 μmol/g. LaMn-RG was the perovskite that had the highest amount of α_2-O_2 desorbed (302.2 μmol/g) followed by YMn-RG (242.2 μmol/g) and PrMn-RG (193.5 μmol/g). The smallest values were obtained on SmMn-RG (151.4 μmol/g) and DyMn-RG (109.6 μmol/g). The evaluation of the α_2-O_2 desorbed is also reported in terms of monolayer, by assuming that one monolayer of oxygen was equal to 4 μmol/m^2, in Table 3. It was found higher than one monolayer for four among the five perovskites under study. Indeed only DyMn-RG presents an amount lower than one monolayer of oxygen (0.86) whereas 1.87 monolayers of oxygen were desorbed on LaMn-RG. These results suggest that the overstoichiometric oxygen of the manganite structure desorbs from the perovskite lattice simultaneously with α_2-O_2 species.

A large difference was also observed concerning the temperature of desorption for the β-O_2 from the bulk of the structure. Indeed the lowest temperature observed for the desorption of those oxygens was on DyMn-RG at 779 °C in comparison with the highest one on YMn-RG at 892 °C. In terms of the amount of β-O_2 desorbed, less than one monolayer was measured for all the catalysts under study. The desorbed amounts were between 142.3 μmol/g on YMn-RG and 51.34 μmol/g on DyMn-RG, which shows large differences in the oxygen mobility in the bulk. Thus, the oxygen mobility in the lattice was found to vary in the following order: YMn-RG < LaMn-RG < PrMn-RG < SmMn-RG < ∩ DyMn-RG.

3.4. Temperature-programmed desorption of CH_3OH (TPD-CH_3OH)

The desorption signals of CH_3OH ($m/z = 31$), CO_2 ($m/z = 44$) and O_2 ($m/z = 32$) during TPD-CH_3OH experiments for the five ground catalysts under study are shown in Figs. 4a–c.

Table 3
Amounts of oxygen desorbed during the TPD-O_2 experiments

Sample	Amount of oxygen desorbed[a]			Number of monolayers desorbed[b]		
	α_1-O_2 (μmol/g)	α_2-O_2 (μmol/g)	β-O_2 (μmol/g)	α_1-O_2	α_2-O_2	β-O_2
LaMn-RG	21.2	302.2	138.0	0.13	1.87	0.84
YMn-RG	19.6	242.2	130.2	0.13	1.64	0.96
PrMn-RG	18.7	193.5	122.8	0.13	1.38	0.87
SmMn-RG	17.0	151.4	67.6	0.13	1.11	0.49
DyMn-RG	16.1	109.6	51.3	0.13	0.86	0.40

[a] Calculated by deconvolution, with Lorentzian fit, of the O_2 desorption curves.
[b] Calculated by assuming 4 μmol/m^2 for one monolayer.

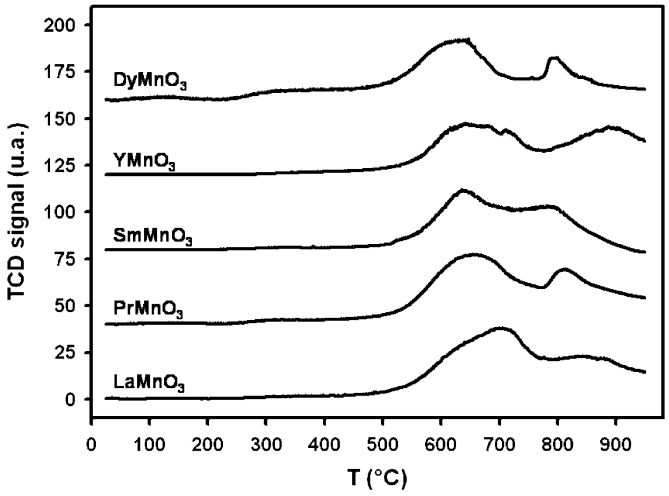

Fig. 3. TPD-O_2 profiles of $AMnO_3$ perovskites.

The catalysts were previously treated under 15% of CH_3OH diluted in He at ambient temperature for 1 h. Fig. 4a displays a major peak centered around 120 °C for each of the five catalysts. This signal is ascribed to a physisorbed methanol phase, which is due to the low temperature of adsorption. On DyMn-RG, a small desorption peak was detected around 500 °C whereas no other significant signal of CH_3OH desorption was detected at higher temperature.

Two kinds of CO_2 desorption signals were detected during the TPD-CH_3OH as shown in Fig. 4b. The first one was detected on each catalyst but at slightly different temperatures and in the following order YMn-RG (246 °C) < DyMn-RG (266 °C) < SmMn-RG (271 °C) < PrMn-RG (285 °C) < LaMn-RG (300 °C). These peaks are the consequence of the total oxidation of CH_3OH, adsorbed on the surface of the perovskites, into CO_2. The second signal of CO_2 was observed at higher temperature and only on YMn-RG (623 °C) and DyMn-RG (613 °C). No significant trace of CO_2 was observed at high temperature on the other perovskites.

The $m/z = 32$ signal was also monitored during these experiments and is shown in Fig. 4c. The low-temperature peaks (below 200 °C) on these five profiles are obviously ascribed to the parent peak of the CH_3OH. The high-temperature peaks (above 600 °C) bear some similarities with the ones observed in TPD-O_2. For LaMn-RG, there was essentially the same pattern as observed during the TPD-O_2 experiment in Fig. 2. Two signals of oxygen were reported, the first at 659 °C, which was ascribed to the α-O_2, and the second at 827 °C, which describes the desorption of β-O_2. On the four other perovskites, only one peak was detected at high temperature. These signals were ascribe to the desorption of β-O_2 as previously observed during the TPD-O_2 experiments. It seems thus that with the exception of LaMn-RG, α-O_2 is essentially consumed by reaction with CH_3OH on all other catalysts.

3.5. Temperature-programmed desorption of CO_2 (TPD-CO_2)

As in the CH_3OH and O_2 desorption experiments, the catalysts were first treated under CO_2 at ambient temperature for 1 h. The MS signal of CO_2 ($m/z = 44$) and O_2 ($m/z = 32$) recorded during the TPD-CO_2 experiments are shown in Figs. 5a and b. As for the TPD-CH_3OH, a signal of CO_2 was detected at low temperature in Fig. 5a. This desorption was found slightly over 300 °C on LaMn-RG and no other signal was detected all along the experiment at higher temperatures. For the other four catalysts, the first peak of CO_2 desorption was located at around 230 °C. Unlike LaMn-RG, a second signal was detected at higher temperatures on these four other catalysts. The temperature of desorption of this peak was in the following order: PrMn-RG (638 °C) < SmMn-RG (662 °C) < YMn (704 °C) < DyMn (715 °C). Concerning the O_2 signal shown in Fig. 5b, the patterns obtained were similar to the ones observed on TPD-O_2. Indeed, two peaks of oxygen desorption, one from the surface (α-O_2) and one from the bulk (β-O_2), can be observed on each profile at the same temperatures as in Fig. 2.

3.6. Catalytic activity in CH_3OH oxidation reaction

The results obtained from catalytic activity tests for the CH_3OH oxidation reaction are presented in Fig. 6. CO_2 was the only product detected in this reaction with no trace of other species, such as formaldehyde or carbon monoxide. The evaluation of catalytic activity of the five catalysts under study was found to vary in the following order: LaMn-RG < YMn-RG < PrMn-RG < SmMn-RG < DyMn-RG. With the exception of the DyMn-RG catalyst, which presents a very poor efficiency, only a very small difference was observed on the four other catalysts. Indeed the temperature at 50% of conversion varied of only several degrees from 163 °C on LaMn-RG to 178 °C on SmMn-RG. At total conversion of methanol, the differences between the four best catalysts were more noticeable and remained in the same order: LaMn-RG (200 °C) < YMn-RG (215 °C) < PrMn-RG (238 °C) < SmMn-RG (245 °C) < DyMn-RG (264 °C). No significant decrease of the specific surface area was measured on each catalyst after the methanol oxidation test.

4. Discussion

The TPR-H_2 experiments reveal an overstoichiometric H_2 uptake on each of the five catalysts under study. Moreover, the

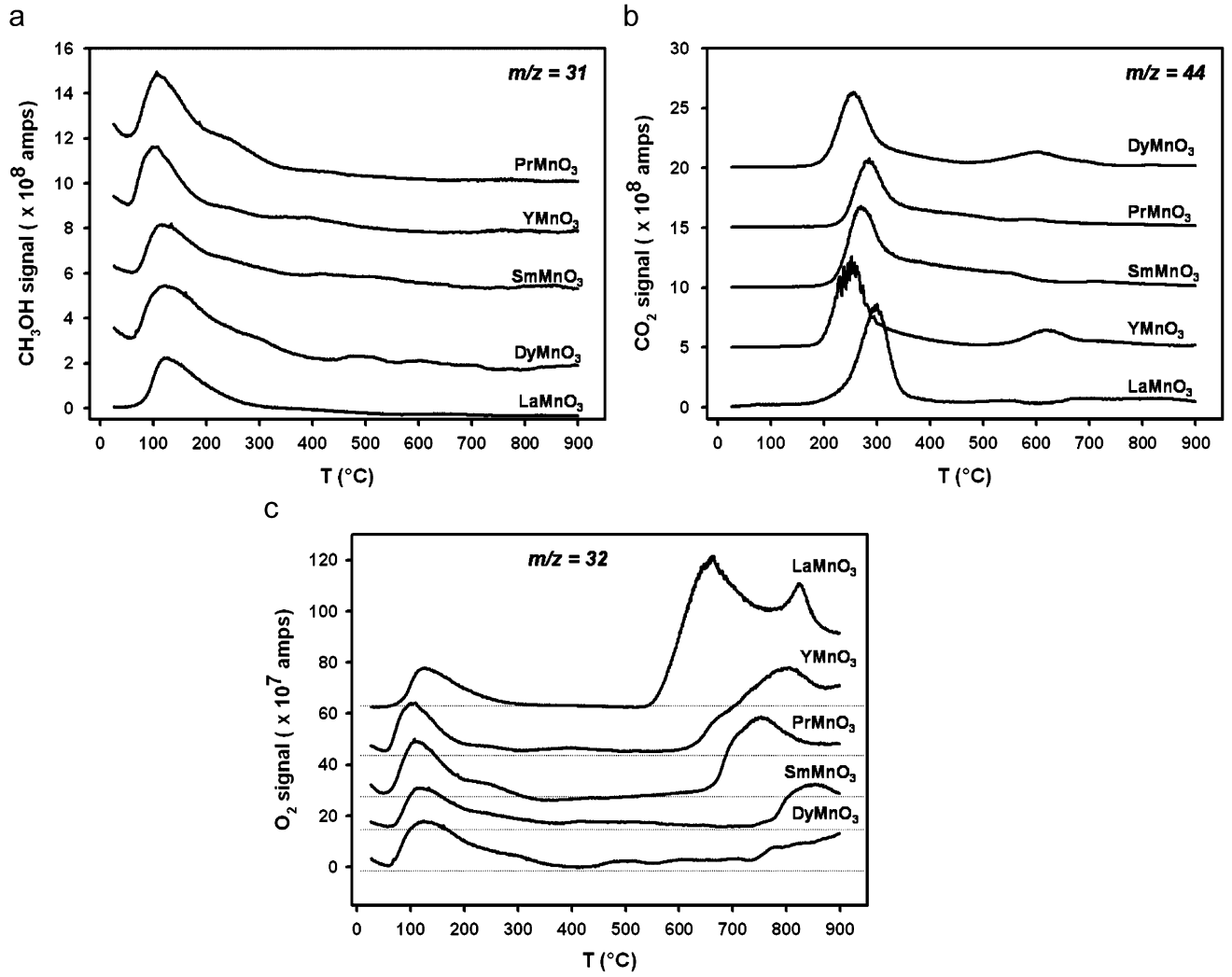

Fig. 4. TPD-CH_3OH profiles of $AMnO_3$ perovkites. MS signal of (a) CH_3OH, (b) CO_2 and (c) O_2.

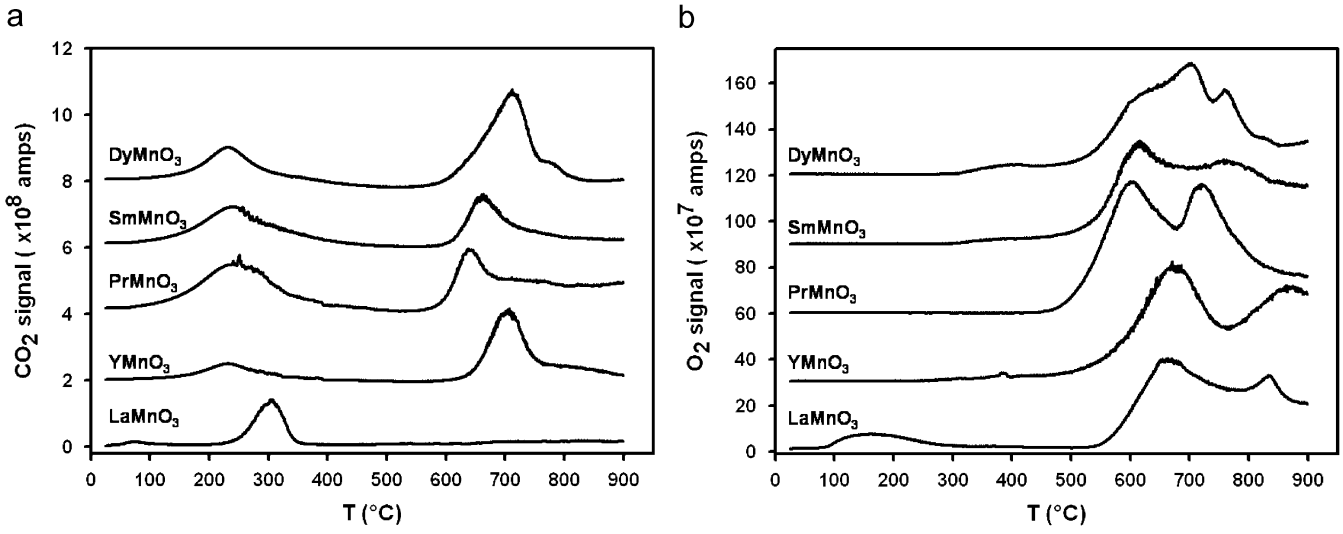

Fig. 5. TPD-CO_2 profiles of $AMnO_3$ perovkites. MS signal of (a) CO_2 and (b) O_2.

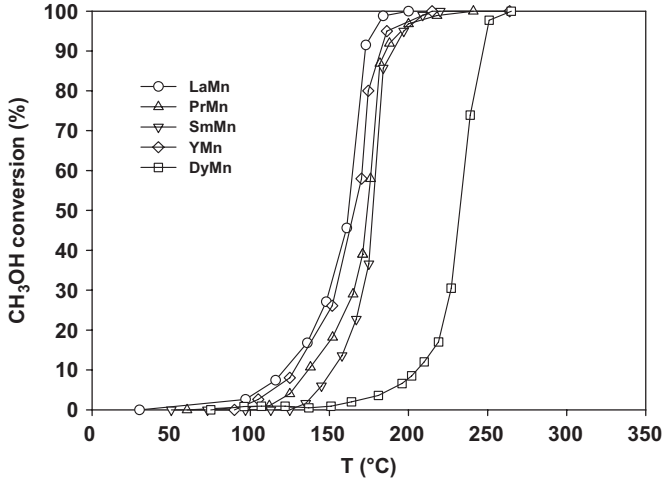

Fig. 6. CH_3OH conversion (VHSV = 22,500 h^{-1}) over $AMnO_3$ perovskites synthetized by reactive grinding.

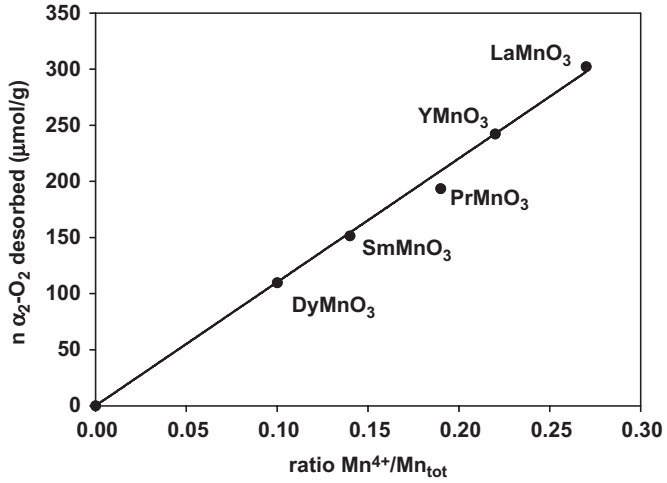

Fig. 7. Correlation between $n(\alpha_2\text{-}O_2)$ desorbed and the amount of Mn^{4+} in the $AMnO_3$ perovskite structure.

presence of a shoulder at low temperature before the main signal of reduction may indicate the reduction of Mn^{4+} species. This induces some modifications to the structure, in particular of the nature of the oxygen in the solid. Even if the reduction of the metallic cation does not occur at the same temperature, no clear effect from the rare earth was evidenced. This may indicate that a combination of both structural and electronic effects may modify the temperature at which the reduction mechanism occurs.

Fig. 7 shows the strong correlation between the amount of $\alpha_2\text{-}O_2$ desorbed and the amount of $Mn^{(IV)}$ species evaluated from the deconvolution of the first manganese reduction signal at low temperature. This correlation is materialized by a linear curve, which crosses the origin of the graph. Moreover, since the amount of $\alpha_2\text{-}O_2$ desorbed is higher than a monolayer, this $\alpha_2\text{-}O_2$ cannot only be a surface species. These two results suggest that $\alpha_2\text{-}O_2$ is indeed the overstoichiometric oxygen. This had already been suggested by us as a result of a study of $LaMn_xCu_{1-x}O_3$ perovskites [33]. However, the large difference observed between the overstoichiometric oxygen evaluated from H_2-TPR (Table 2) and the $\alpha_2\text{-}O_2$ desorbed (Table 3) is still puzzling. It might be that only a fraction of overstoichiometric oxygen detected in H_2-TPR evolves as a $\alpha_2\text{-}O_2$ desorption peak. Some overstoichiometric oxygen may desorb at higher temperature and in part with the $\beta\text{-}O_2$ peak.

Based on the results obtained during the TPD-O_2 experiments, some correlations are suggested in Fig. 8a–d. Temperature of desorption and amounts of α_1- α_2- and $\beta\text{-}O_2$ desorbed were investigated as functions of different parameters. The temperature of desorption of $\alpha_2\text{-}O_2$ seems to be closely related to the electronegativity of the rare earth in the perovskite structure. Indeed, Fig. 8a clearly shows that the $\alpha_2\text{-}O_2$ desorption temperature increases as the electronegativity of the *A*-site cation decreases. This indicates that the ionic nature of the bonds Mn–O and A–O plays a significant role in the release of overstoichiometric oxygen. The difference in electronegativity ($\Delta\chi$) between the manganese (1.5 in the Pauling scale) and the rare earth may be responsible for the evolution of the ionic nature of the bond. The higher the $\Delta\chi$ is, the higher the electrons would be attracted by the Mn^{3+}. This allows the Mn^{3+} to compensate for the attraction of its electrons to the O_2^- species (Eqs. (1) and (2)). Thus, the $\alpha_2\text{-}O_2$ desorption may be easier when the $\Delta\chi$ is low. Such electronic interactions may explain the differences observed in the $\alpha_2\text{-}O_2$ desorption temperature in Fig. 3. Concerning the $\alpha_1\text{-}O_2$ desorbed, it was unsurprisingly found to vary with the specific surface area (S_{BET}), Fig. 8b. The total amount of $\alpha\text{-}O_2$ desorbed increases with the specific surface area. LaMn-RG, which presents the highest specific surface area, is also the catalyst, which displays the highest total amount of $\alpha_1\text{-}O_2$ desorbed during the TPD-O_2 experiment.

A correlation was also found between the desorption temperature of the $\beta\text{-}O_2$ from the bulk of the structure and the density of the rare-earth simple oxide A_2O_3. The density was chosen due to the specificity of the rare earths from the lanthanum family particularly because of their ionic radius, which decreases with the increase of the atomic number. The density of the oxide allows therefore to take into account both structural and electronic interactions of the A^{3+} cation and the O^{2-} anions in the structure. Fig. 8c clearly shows good correlation between the intrinsic density of the A^{3+} rare-earth cation oxide and the $\beta\text{-}O_2$ desorption temperature. The A^{3+} rare-earth oxide with elevated density as observed on SmMn-RG or DyMn-RG with, respectively, 8.35 and 7.81 g/cm^3 may allow the shifting of the desorption signal to the lower temperatures compared with the solids formed with lower density A^{3+} cation like LaMn-RG (6.51 g/cm^3) and YMn-RG (5.01 g/cm^3). Such a correlation, which is inversely proportional to the ionic radius, is surprising, but it gives some informations about the large impact of the electronic atomic interactions induced by the rare earth in the perovskite structure.

Finally, the amount of $\beta\text{-}O_2$ was correlated with the ratio S_{th}/S_{BET}, which reflects the densification of perovskite particles and also the surface occupied by the grain boundaries (S_{gb}) in Fig. 8d. Thus, the amount desorbed at high temperature was found to increase when the density of the structure (which increases when S_{th}/S_{BET} increases) and the surface area of grain boundaries (S_{gb}) decrease. This may indicate that elevated S_{gb} prevents the oxygen transfer from the bulk to the surface since the formation o f $\beta\text{-}O_2$ desorption site does not occur in amorphous grain boundaries (Eq. (3)). On the contrary, the oxygen transfer through the crystal may be less affected on the catalysts that present small grain boundary surface area as observed on YMn-RG and LaMn-RG.

The electronegativity seems to also play a role in the desorption of CO_2 during TPD-CH_3OH and TPD-CO_2 (Fig. 9). As observed in a previous work, the desorption of CO_2 at low

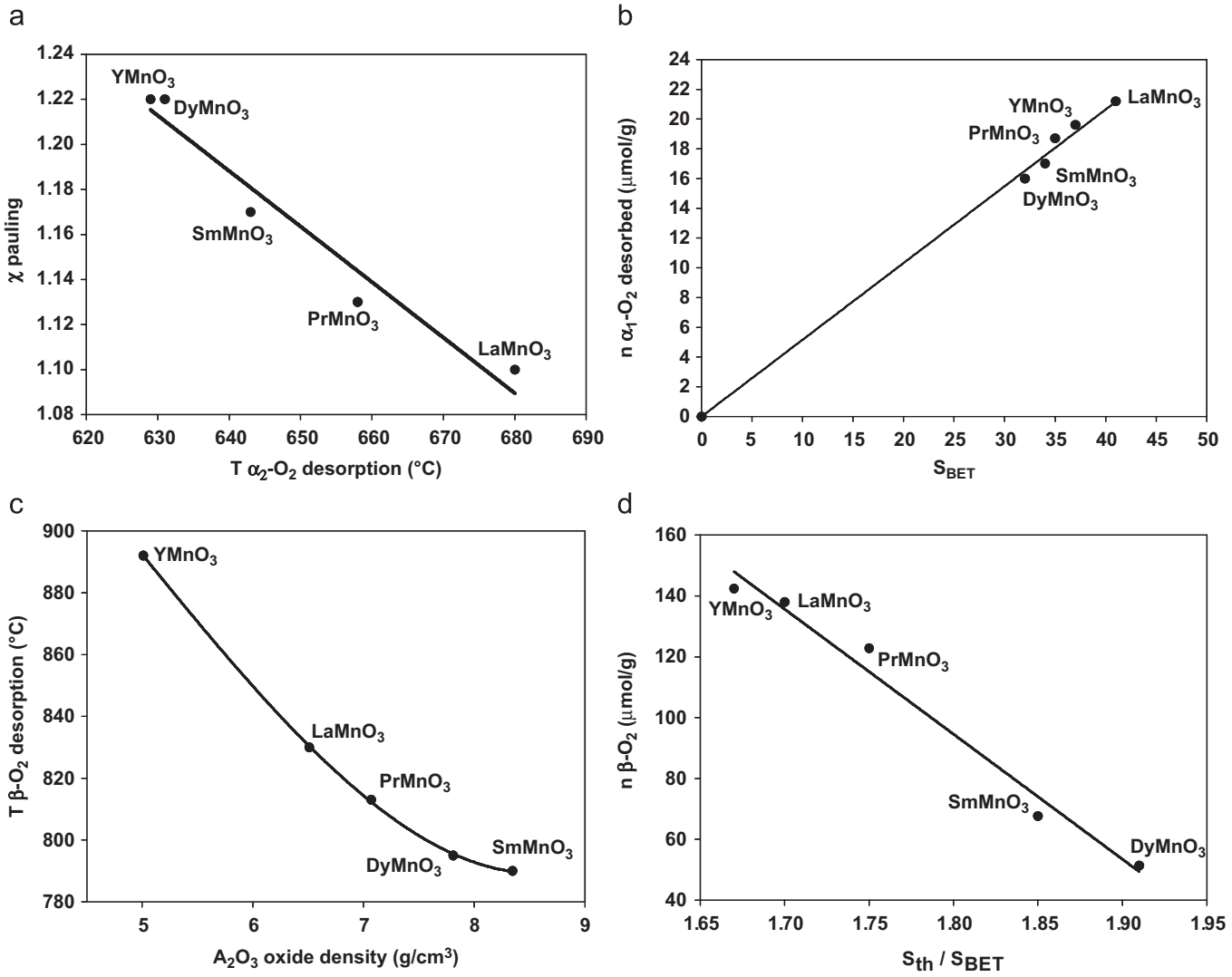

Fig. 8. Correlation between oxygen desorption properties and electronical and structural properties of the $AMnO_3$ perovskites.

temperature may occur according to Eq. (5) [32,34,35]:

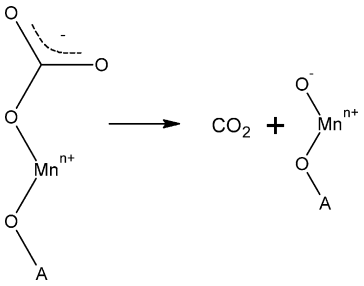

(5)

A change in the nature of the rare earth may induce a change in the polarity of the bonds between oxygen and the *A*-site cation and the transition metal cation. Similar to what was deduced from the TPD-O_2 experiments (Fig. 8a), the difference in electronegativity between both cations was closely related with the stability of the monodentate carbonate (Eq. (5)). Indeed the increase of this difference may lead to an increase of the δ- on the active site $Mn^{n+}O^{-}$ by attraction of the electrons of the bond A–O–Mn. This may generate an increase in basic strength of the site, which may induce the stabilization of the monodentate carbonate. Due to the electronegativity of Mn (1.5 in the Pauling scale) an increased electronegativity difference corresponds to A elements with lower electronegativity. This may explain the rather high temperature at which this type of carbonates was desorbed from LaMn-RG since La is the less electronegative element of the five rare earths under study. Thus, the temperature of desorption of CO_2 after chemisorption (TPD-CO_2) or reaction (TPD-CH_3OH) may be directly related to the electronegativity of the rare earth. A gap of 20 °C is systematically observed on CO_2 desorption temperature between CO_2- and CH_3OH-TPD experiments. Such a difference may be due to the basicity induced by the presence of methanol adsorbed on the surface of the catalysts during TPD-CH_3OH. A stronger basicity of the surface leads to the stabilization of the carbonates and as a consequence a higher temperature is required to allow their desorptions.

At higher temperatures, the desorption of the CO_2 during the TPD-CH_3OH experiments was found to be highly related to the total amount of α-O_2 available [32]. On the five perovskites under study, the total amount of α-O_2 available was higher (over 1.20 monolayers except for DyMn-RG) than the one observed on $LaCoO_3$ or $LaFeO_3$ (below 1.20 monolayers) catalysts in our previous work so that this explains the small (DyMn-RG) or the absence of such signals [32]. In the case of the TPD-CO_2 (Fig. 4), a second signal that is ascribed to the bidentate carbonates was noticed around 600 °C. However, it was surprising to observe that during TPD-CH_3OH the second signal of CO_2 (Fig. 5a) and the peaks ascribed to the desorption of α-O_2 (Fig. 5b) were detected at the same temperature. This observation shows the reversibility of the adsorption/desorption of the bidentate carbonate species

since the desorption of α-O_2 is a reversible process [32,34,35]:

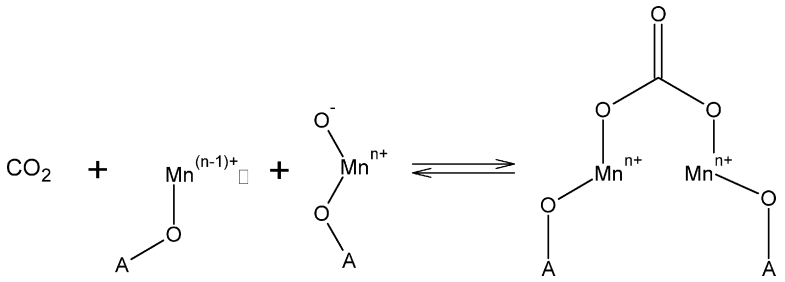

(6)

Moreover, the signal of oxygen evolving above 750 °C and ascribed to oxygen from the bulk, observed on each catalyst (Fig. 5b), is another proof of the reversibility of this process since β-O_2 desorption is not affected by the formation of bidentate carbonates.

Based on CH_3OH- and CO_2-TPD, a multiple step mechanism was suggested for the methanol oxidation reaction [32]. After adsorption of the methoxide species on an anion vacancy (Eq. (7)), a first oxidation leads to the formation of a hypothetical "bi-oxidized" intermediate (Eq. (8)) [32,36,37]:

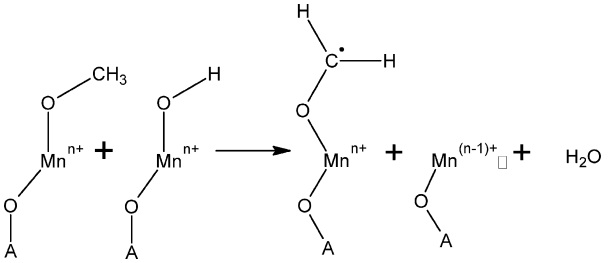

(7)

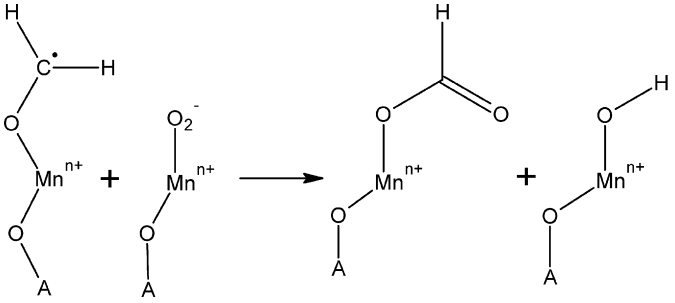

(8)

Two ways were suggested depending on the total amount of α-O_2 available. As long as the surface oxygen density is sufficient, a second oxidation step leads to the formation of the monodentate carbonate (Eq. (9)) [32]:

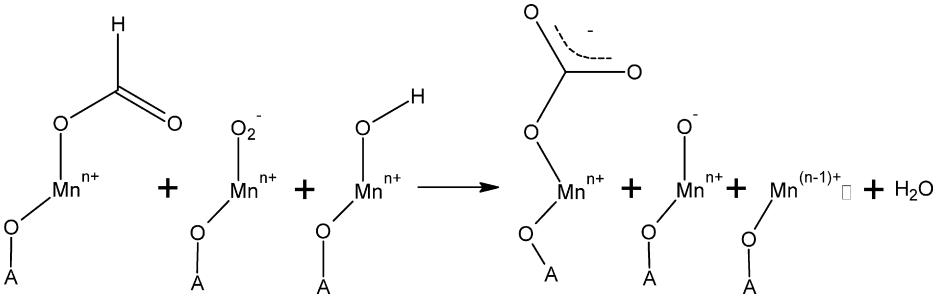

(9)

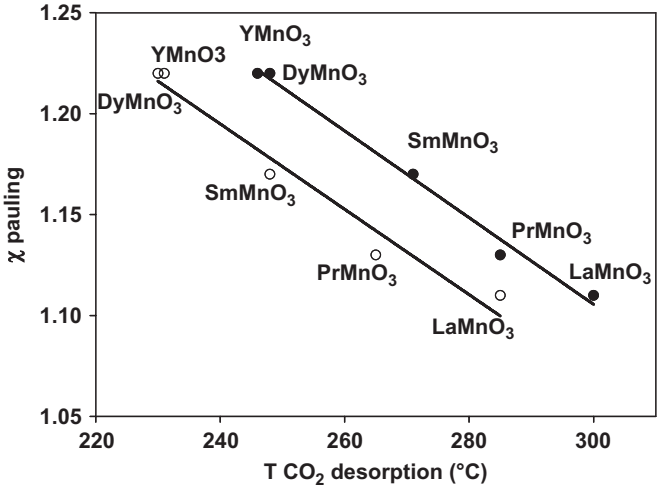

Fig. 9. Correlation between electronegativity of the rare earth in the $AMnO_3$ perovskites and desorption temperature of the monodentate carbonates during TPD-CH_3OH (●) and TPD-CO_2 (○).

In accordance with TPD-CH_3OH and TPD-CO_2, carbon dioxide is produced by desorption from the monodentate carbonate (Eq. (5)). By contrast in case of a lack of α-O_2, another reaction that leads to the bidentate carbonate occurs (Eq. (10)):

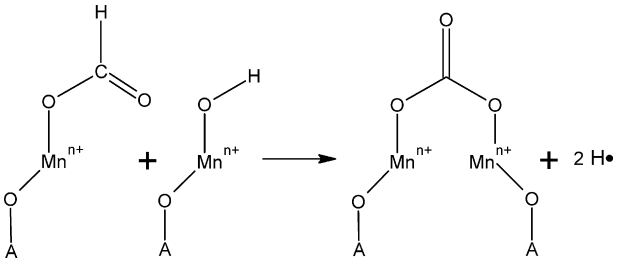

(10)

With the exception of the DyMn-RG catalysts the catalytic tests for the methanol oxidation, presented in Fig. 6, show only small differences. Reducibility and α-O_2 availability at the surface of the catalysts were identified as the major factors for the total

oxidation of methanol into CO_2 [32]. Indeed the efficiency in this oxidation was found to be improved when α-O_2 is available. The catalysts are ranked in terms of efficiency, and also in terms of total amounts of α-O_2 desorbed, in the following order: LaMn-RG > YMn-RG > PrMn-RG > SmMn-RG > DyMn-RG. The large difference in activity between DyMn-RG and the other ground perovskites is attributed to its low reducibility (Table 2) but also to a rapid formation of bidentate carbonates (Eq. (10)). According to the suggested mechanism the formation of bidentate carbonates is related to a lack of the α-O_2 available to achieve the complete oxidation (Eq. (9)). Such a formation may cause the active oxidation sites to become inaccessible. In opposition to the formation of monodentate carbonates, which desorb at lower temperature, the accumulation of bidentate carbonates is more detrimental. Indeed at the temperature at which the oxidation of methanol into CO_2 occurs, the bidentate carbonates remain adsorbed on the surface of the perovskite, since according to the TPD-CH_3OH and TPD-CO_2, the desorption temperature of those carbonates requires higher temperature. This may explain the slow oxidation rate of the DyMn-RG considering its weak density of surface and grain boundary oxygen. Thus, a lack of α-O_2 available is directly related to the formation of bidentate carbonates and to the weak activity at low temperature. For the four other catalysts, which present a higher density of surface and grain boundary oxygen, the formation of monodentate carbonates by oxidation of the hypothetical "bi-oxidised" intermediates (Eq. (9)) is the major way suggested in comparison with the formation of the bidentate carbonates species (Eq. (10)).

5. Conclusion

The presence of a Mn^{4+} species on each perovskite was quantified based on the H_2 uptake during the TPR experiments. In spite of some differences in the reducibility behaviour of $AMnO_3$ perovskites, the relation with the nature of the rare earth in the perovskite has not been fully elaborated and is still unclear. The amount of $Mn^{(IV)}$ in the $AMnO_3$ perovskite was however found to be closely correlated with the amount of α_2-O_2 desorbed. Moreover, the amount desorbed, which exceeds the monolayer, and the linear correlation observed with the $Mn^{(IV)}/Mn_{tot}$ ratio suggest the overstoichiometric nature of these oxygens. Concerning the TPD-O_2, the influence of the rare earth was correlated with several intrinsic properties of the *A*-site cation. Temperatures of oxygen desorption were found to be directly related to the electronegativity of the rare earth for α_2-O_2 whereas the density of the rare-earth oxide was found to be the meaningful parameter for the β-O_2 desorption temperature. The effects induced by the nature of the A cation were indirectly linked with the amount of oxygen desorbed. Indeed the density of surface oxygen was unsurprisingly found to be related to the specific surface area. Concerning the β-O_2, a correlation with the ratio S_{th}/S_{BET} was found. This indicates that the nature of the rare earth affects the state of aggregation of elementary perovskite particles. Both TPD-CH_3OH and TPD-CO_2 experiments show the same order in stability of the monodentate carbonates, reflected by their order of desorption temperatures. This stability was found to be highly related with the electronegativity of the rare earth. Indeed the lower the electronegativity, the more the active sites are basic, which means that the carbon dioxide is desorbed at higher temperatures.

In accordance with our previous study, the mechanism of methanol oxidation varies depending on the α_2-O_2 concentration. A high density leads to the total oxidation by the formation of monodentate carbonates, which are desorbed at low temperatures. In contrast, a low α_2-O_2 density leads to the formation of bidentate carbonates, which, due to their higher temperature of desorption, may induce a deactivation process by competing with oxygen for oxygen vacancies (Eq. (6)). Even if slight differences were found in the activity for methanol oxidation (excluding DyMn-RG), the nature of the *A*-site cation was related with these differences in a complex manner. Indeed the rate of methanol oxidation should be related with S_{BET}, which depends on the nature of the rare earth for a given preparation procedure. As indicated by the results in Fig. 8b, the surface concentration of α_1-O_2 does not seem to be affected by the nature of the rare earth. Thus, at high enough gas-phase oxygen concentrations (such as the 5% O_2 used in the methanol oxidation tests), the observed oxidation rates are only dependent on S_{BET}. The small differences (between 32 and 41 m^2/g) in S_{BET} explain the small differences observed in methanol conversions (Fig. 6). Thus, the direct effects of the electronegativity of the rare earth and the induced basicity of the active oxygen (see Eq. (5)) on methanol oxidation rate are not very significant as long as deactivation by bidentate carbonates is not involved. In the case of accumulation of bidentate carbonates at low gas-phase oxygen concentration, an increase in the reaction temperature over 650 °C is required for the desorption of these species.

Acknowledgments

Nanox Inc. (Québec, Canada) is acknowledged for the preparation of the RG samples. The financial contribution of the Natural Sciences and Engineering Council of Canada, through an industrial chair, is gratefully acknowledged.

Appendix A. Supplementary data

Supplementary data associated with this article can be found in the online version at doi:10.1016/j.jssc.2008.07.029

References

[1] W.F. Libby, Science 171 (1971) 499.
[2] R.J.H. Voorhoeve, J.P. Remeika Jr., P.E. Freeland, B.T. Mathias, Science 177 (1972) 353.
[3] R.J.H. Voorhoeve, D.W. Johnson, J.P. Remeika, P.K. Gallagher, Science 195 (1977) 827.
[4] R.J.H. Voorhoeve, in: H.H. Burton, R.L. Garden (Eds.), Advanced Materials in Catalysis, Academic Press, New York, 1977, p. 127.
[5] L.G. Tejuca, J.L.G. Fierro, Properties and Applications of Perovskite-type oxides, Dekker, New York, 1993.
[6] H. Arai, T. Yamada, K. Eguchi, T. Seiyama, Appl. Catal. 26 (1986) 265.
[7] P.K. Gallagher, Mater. Res. Bull. 3 (1967) 225.
[8] H.-M. Zhang, Y. Teraoka, N. Yamazoe, Chem. Lett. (1987) 665.
[9] J. Kirchnerova, D. Klvana, Int. J. Hydrogen Energy 19 (1994) 501.
[10] R.A.M. Giacomuzzi, M. Portinari, I. Rossetti, L. Forni, Stud. Surf. Sci. Catal. 130 (2000) 197.
[11] S. Kaliaguine, A. van Neste, US Patent 6017504, 2000.
[12] S. Kaliaguine, A. Van Neste, V. Szabo, J.E. Gallot, M. Bassir, R. Muzychuk, Appl. Catal. A 209 (2001) 345.
[13] T. Nitadori, T. Ichiki, M. Misono, Bull. Chem. Soc. Jpn. 61 (1988) 621.
[14] O. Parkash, P. Ganguly, G.R. Rao, C.N.R. Rao, D.S. Rajoria, V.G. Hide, Mater. Res. Bull. 9 (1974) 1173.
[15] P.E. Marti, A. Baiker, Catal. Lett. 26 (1994) 71.
[16] P. Ciambelli, S. Cimino, S. De Rossi, M. Faticanti, L. Lisi, G. Minelli, I. Pettiti, P. Porta, G. Russo, M. Turco, Appl. Catal. B: Environ. 24 (2000) 243.
[17] M. Alifanti, R. Auer, J. Kirchnerova, F. Thyrion, P. Grange, B. Delmon, Appl. Catal. B: Environ. 41 (2003) 71.
[18] R.W. McCabe, P.J. Mitchell, Appl. Catal. 27 (1986) 83.
[19] H.K. Plummer Jr., W.L.H. Watkins, H.S. Ghandi, Appl. Catal. 29 (1987) 261.
[20] J.S. Chung, R. Miranda, C.O. Bennett, J. Catal. 114 (1988) 398.
[21] P. Forzatti, E. Tronconi, G. Busca, Appl. Catal. A: Gen. 157 (1997) 387.
[22] V. Lochar, J. Machek, J. Tichy, Appl. Catal. A: Gen. 228 (2002) 95.
[23] M. Brandhorst, S. Cristol, M. Capron, C. Dujardin, H. Vezin, G. Le bourdon, E. Payen, Catal. Today 113 (2006) 34.
[24] T. Arakawa, S.I. Tsuchi-Ya, J. Shiokawa, J. Catal. 74 (1982) 317.
[25] T. Arakawa, N. Ohara, H. Kurachi, J. Shiokawa, J. Colloid Interf. Sci. 108 (1985) 407.

[26] B.C. Tofield, W.R. Scott, J. Solid State Chem. 10 (1974) 183.
[27] J.M.A. Van Roosmalen, E.H.P. Cordfunke, R.B. Helmholdt, H.W. Zandbergen, J. Solid State Chem. 110 (1994) 320.
[28] S. Royer, F. Bérubé, S. Kaliaguine, Appl. Catal. A 282 (2005) 273.
[29] S. Royer, A. Van Neste, R. Davidson, S. McIntyre, S. Kaliaguine, Ind. Eng. Chem. Res. 43 (2004) 5670.
[30] S. Royer, H. Alamdari, D. Duprez, S. Kaliaguine, Appl. Catal. B 58 (2005) 275.
[31] L. Lisi, G. Bagnasco, P. Ciambelli, S. De Rossi, P. Porta, G. Russo, M. Turco, J. Solid State Chem. 146 (1999) 176.
[32] B. Levasseur, S. Kaliaguine, Appl. Catal. A: Gen. 343 (2008) 29.
[33] R. Zhang, A. Villanueva, H. Alamdari, S. Kaliaguine, Appl. Catal. A 307 (2006) 85.
[34] L.G. Tejuca, C.H. Rochester, J.L.G. Fierro, J.M.D. Tascon, J. Chem. Soc. Faraday Trans. I 80 (1984) 1089.
[35] M.A. Pena, J.L.G. Fierro, Chem. Rev. 101 (2001) 1981.
[36] J.F. Edwards, G.L. Schrader, J. Phys. Chem. 89 (1985) 782.
[37] F. Ouyang, S. Yao, K. Tabata, E. Suzuki, Appl. Surf. Sci. 158 (2000) 28.